CZASOPISMO TECHNICZNE M
WYDAWNICTWO POLITECHNIKI KRAKOWSKIEJ

z. 5-M/2008
ISSN 0011-4561
ISSN 1897-6328

JOCHEN GRÜNIG, MATTHIAS KRAUME*

FILM FLOW ON A VERTICAL WIRE – EXPERIMENTAL INVESTIGATION OF FLUID DYNAMICS AND MASS TRANSFER

SPŁYW FILMU WZDŁUŻ PIONOWEGO PRZEWODU – BADANIA EKSPERYMENTALNE DYNAMIKI PRZEPŁYWU I TRANSPORTU MASY

Abstract

Liquid is supplied at the top of a vertical wire and runs down as annular liquid film while gas is flowing in counter current. The film flow distinguishes a thin basis film and fast moving drop-shaped beads. Experiments were carried out to examine the local film thickness of water and ethanol and the mass transfer of ethanol at ambient conditions. Here, the varied parameters were the gas and liquid load. Water showed a thinner basis film and larger beads, which indicated the influence of the higher surface tension compared to ethanol. The mass transfer measurements pointed out, that the liquid load has a effect on the mass transfer due to the changing film structure.

Keywords: wetted wire, falling film, film thickness, mass transfer

Streszczenie

Ciecz spływa pierścieniową warstwą filmu wzdłuż pionowego przewodu, w przeciwprądzie do gazu. W spływającej cieczy można wyróżnić cienką warstwę filmu i szybko poruszające się krople. Celem badań było ustalenie lokalnej grubości filmu wody oraz etanolu i jego transportu dla różnych wydatków gazu i cieczy. Dla wody charakterystyczne były cieńsza warstwa filmu i większe krople, co wskazuje na wpływ większego napięcia powierzchniowego w porównaniu z etanolem. Badania wskazują, że na transport masy ma wpływ wielkość wydatku cieczy, która zmienia strukturę warstwy filmu.

Słowa kluczowe: zwilżony przewód, spływający film, grubość warstwy filmu, wymiana masy

* Dipl.-Ing. Jochen Grünig, Prof. Dr.-Ing. Matthias Kraume,
Institut für Prozess- und Verfahrenstechnik, Technische Universität Berlin.

1. Introduction

In many technical applications for heat and mass exchange operations, phase contact apparatus are employed. In packed columns for gas/liquid systems, internal packings enlarge the interfacial surface area. The liquid phase wets the packing elements as it flows downwards, while the gas phase generally flows in counter current. Modern packings show high gas- and liquid loads at moderate specific pressure drop. However, the liquid tends to develop an uneven distribution in the packing due to wall effects and the formation of rivulets. Thus, the liquid has to be collected and redistributed after a certain column height.

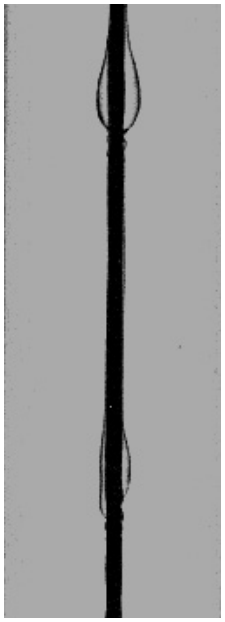

Fig. 1. Film structure

Rys. 1. Struktura spływu

A new packing concept is expected to have some advantages compared to conventional packings available today. This new packing mainly consists of bundles of parallel vertical wires. Each wire is supplied with liquid separately at the top by special liquid distributor elements. The liquid runs down and coats the wires as thin annular film. Because the liquid stays at the wires during its passage through the column, the liquid distribution should be uniform across the whole column height and the liquid does not need to be redistributed. This saves costs for redistributor internals and overall column height. Furthermore, the specific pressure drop is expected to be low, so this packing concept seems to be suitable especially in applications with large gas flow rates like e.g. flue gas treatment in power plants.

Because of its technical relevance, hydrodynamics and mass transfer of packings and falling films were widely investigated since decades. It is well known, that practically all liquid films form waves that influence fluid dynamics and the mass transfer of the film [1–3]. The presence of a counter current gas flow promotes the formation of waves and at increasing gas velocities, the film thickness rises as interfacial shear forces retard the film flow. At a certain gas velocity, the waves break up and droplets are entrained with the gas flow [4]. In narrow gas channels, witch can be found in falling film evaporator tubes as well as in packed columns, the flooding point is reached, when the liquid does not drain off and fills the gas channels completely [5]. As a result of increasing film thickness at rising liquid load, the gas channels get narrower and therefore the load limits are reached at lower gas loads. Thus, the liquid hold-up, i.e. the total liquid volume in the column, is influenced by both the gas and liquid load [6].

Fluid dynamics of film flow on single wires without counter current gas flow have been investigated by Hattori et al. [7]. It was found, that the film structure consists of a thin basis film, that is overrun by beads of different shape (see Fig. 1). Detailed theoretical analyses of the annular film flow were conducted by e.g. Goren [8], Lin [9], and Trifonov [10]. In their works, they explain the mechanism of the formation of beads due to capillary forces and the influence of the film curvature. Several Authors observed the mass transfer of gas

absorption with single and multiple wire experiments [11–13] and suggested the application of wetted-wire columns for the separation of CO_2 from flue gas.

To understand the physical phenomena of the two-phase flow and to estimate the performance of the packing, the film flow on a single vertical wire has been observed.

2. Methods and materials

The wire was fed with a constant liquid flow at the upper end, so an annular liquid film sheaths the surface and flows down. Air is directed in counter current to the liquid flow. The tested liquids were water and ethanol with the physical properties given in Table 1. These liquids were chosen because of a wide difference in their surface tension σ, while the other relevant physical properties are similar. Water was purified in a reverse osmosis system, ethanol was of synthesis quality.

Table 1

Physical properties of the tested liquids at 20°C [14, 15]

	[kg/m^3]	[mPa s]	[N/m]
water	998	1,0	72,74
ethanol	810	1,2	23,03

A flow sheet of the test facility is shown in Fig. 2. A more detailed description of the plant was presented in previous papers [16, 17]. The wire (stainless steel, 1 mm OD) is clamped centered in a vertical glass channel with a rectangular cross section area of 20×20 mm and a length of 1000 mm (1). The liquid is supplied to the wire at the upper end by a coaxial tube with an inner diameter of 2 mm. At the lower end, a coaxial glass tube (15 mm ID) collects the liquid, which is then directed into a sample tank (4). The weight of the sample tank is recorded on computer by an electronic balance. A gear type pump (5) recycles the liquid via a buffer tank back to the wire. To reduce fluctuations in the liquid flow rate, a buffer tank (6) is installed behind the pump. A constant outlet flow rate is obtained, when the liquid level in the buffer tank is steady.

The air was filtered and decompressed to system pressure, a rotameter was used to meter the volume flow. It enters the channel at the bottom and is released into the environment at the top.

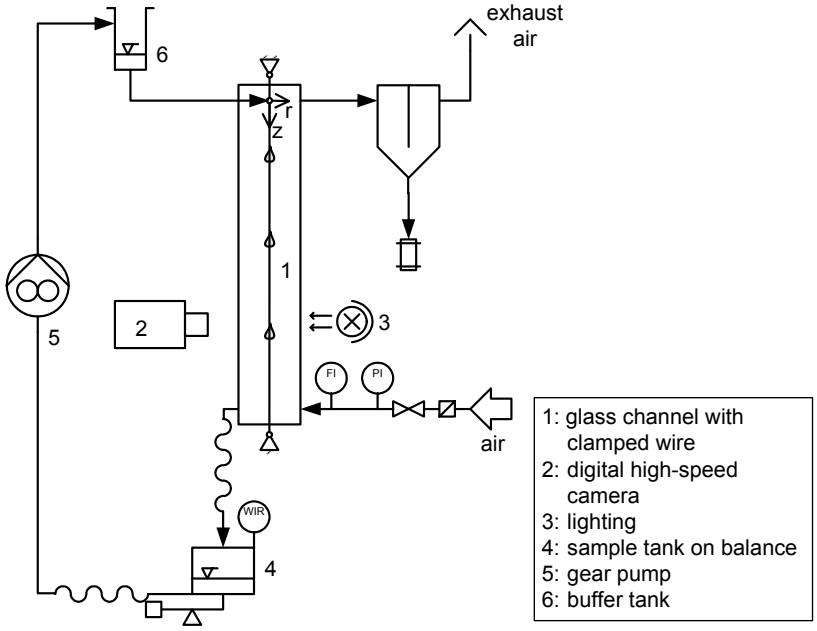

Fig. 2. Flow sheet of the test facility

Rys. 2. Schemat stanowiska badawczego

2.1. Film thickness

The film thickness and the bead velocity are measured with a high speed camera (Photonfocus MV-D752-160-CL-8, 350 fps @ 752 × 582 pixels, 256 grayscales). The camera is installed at a wire length of z = 730 mm. A pulsed synchronized LED element (CCS LND-300A-DF) is mounted at the channel as back lighting. A similar technique for film thickness measurements on the inside of tubes is used by Karimi and Kawaji [18]. For the film thickness measurements, a magnifying telecentric objective (Sil Correctal T/3.0) was used. Digital image sequences were recorded on computer with a framegrabber bus card (Silicon Software GmbH, mircoEnable III).

An image processing software (ImageProPlus®) is used to identify the film as object in the image sequences. Parts of the film appear as dark areas in the pictures, so that the corresponding objects can be detected by adjusting a region of grayscales. As an example, this procedure is illustrated in Fig. 3 for the film thickness measurements. A picture of the sequence shows the wire in the middle as dark region with the film boundary appearing as thin dark line on both sides.

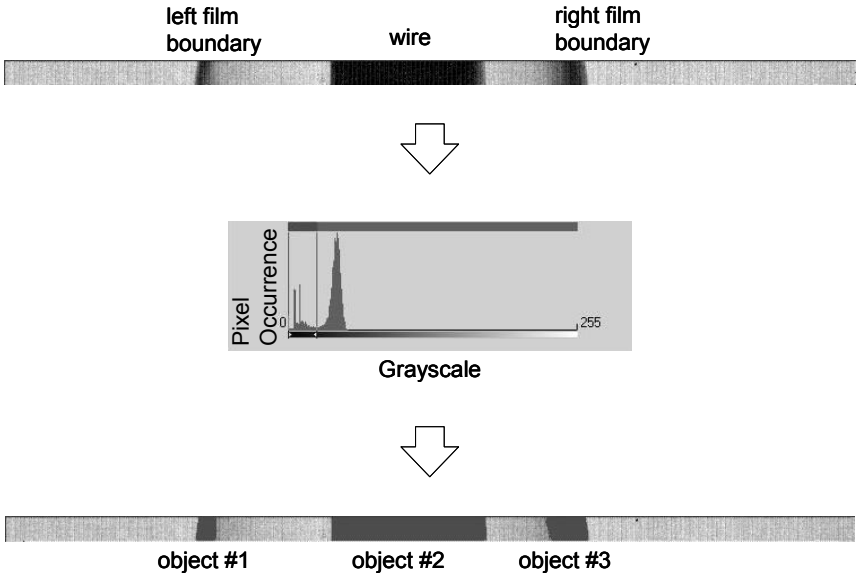

Fig. 3. Object recognition with grayscale analysis in ImageProPlus®

Rys. 3. Identyfikacja na podstawie analizy szarości w ImageProPlus®

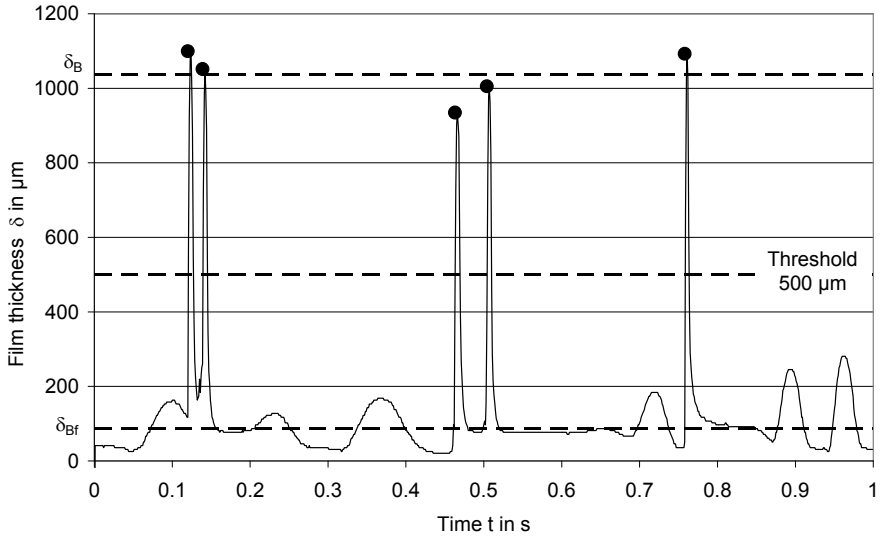

Fig. 4. Time-dependent local film thickness; threshold value, mean bead thickness δ_B and mean basis film thickness δ_{Bf}

Rys. 4. Zależność lokalnej grubości filmu od czasu, wartość progowa, średnia wielkość kropli δ_B i średnia bazowa grubość filmu δ_{Bf}

The object recognition toolbox of the ImageProPlus® software is able to display the grayscale spectrum of the picture and allows marking a grayscale range. Objects are build from adjacent pixels in this range after certain rules, and the user can give additional limits for object exclusion, such as area or size of the objects. This procedure is done for all pictures in a sequence and the respective size and position of the objects are recorded in a table in the spreadsheet software MS Excel®. With the data of the outmost objects and a scale (the diameter of the dry wire), the film thickness can be determined in every picture of the sequence. Thus, the time dependent local film thickness can be displayed as shown in Fig. 4. In the evaluation, a threshold value of 500 µm is introduced to distinguish between the mean bead thickness δ_B and the mean basis film thickness. The image sequences were recorded with a frame rate of 1000 fps in a time interval of 10 s. The evaluated data showed up to 40% deviation from the mean values, which indicates the strong irregularity of the flow structure.

2.2. Gas side mass transfer

For mass transfer measurements, the decline of the liquid mass in the cycle due to evaporation was observed by recording the weight of the sample tank with the time. It was the aim to find the gas side mass transfer coefficient β_g, which is defined as

$$\beta_g = \frac{\dot{N}_A}{A_W \cdot \Delta c_{A,\ln}} \tag{1}$$

where $\dot{N}_\mathrm{A} = \dot{M}_\mathrm{A} / \tilde{M}_\mathrm{A}$ is the molar flow rate, $A_\mathrm{W} = \pi \cdot d_\mathrm{W} \cdot L_\mathrm{W}$ is the area of the wire surface, and $\Delta c_{A,ln}$ is the logarithmic concentration difference. Only ethanol was used as liquid, because the gas inlet concentration of ethanol could be assumed to be zero. Thus, the logarithmic concentration difference can be described as

$$\Delta c_{A,ln} = \frac{c_{A,out}}{\dfrac{c_{A0}}{c_{A0} - c_{A,out}}} \tag{2}$$

In this definition, c_{A0} is the equilibrium concentration of component A (ethanol) at the liquid/gas interface and $c_{A,out}$ is the concentration of component A in the gas phase at the outlet of the channel. The outlet concentration is determined with the transferred mass flow rate $\dot{M}_A$ and the gas flow rate $\dot{V}_A$ in the channel, while its increase by the evaporated liquid has been neglected

$$c_{A,out} = \frac{\dot{M}_A}{\tilde{M}_A \cdot \dot{V}_g} \tag{3}$$

To calculate the equilibrium concentration, the ideal gas law was used

$$c_{A0} = \frac{p_\mathrm{S}}{R \cdot T} \tag{4}$$

Herein $p_S = 58{,}7$ hPa is the saturation pressure of ethanol at ambient temperature $T = 293{,}15$ K.

Braun and Hiby studied the gas side mass transfer of falling films on the inside of tubes with co and counter current gas flow [3]. They found an empirical equation for the gas side mass transfer for counter current gas flow

$$\mathrm{Sh}_g = 0{,}015 \cdot \mathrm{Re}_g^{0,75} \cdot \mathrm{Re}_l^{0,16} \cdot \mathrm{Sc}_g^{0,44} \cdot \left[1 + 5{,}2 \cdot (L_T / d_T)^{-0,75}\right] \tag{5}$$

In this equation, L_T and d_T are the length respectively the diameter of the tube. The dimensionless groups are defined as follows

$$\mathrm{Sh}_g = \frac{\beta_g \cdot d_T}{D_g} \qquad \mathrm{Re}_l = \frac{\dot{V}_l}{d_T \cdot \pi \cdot \nu_l} \qquad \mathrm{Re}_g = \frac{4 \cdot \dot{V}_g}{d_T \cdot \pi \cdot \nu_g} \qquad \mathrm{Sc}_g = \frac{\nu_g}{D_g} \tag{6}$$

For the comparison with the experimental data, in Eq. (5) the length L_T and diameter d_T of the tube were replaced by the length and hydraulic diameter of the channel. For the calculations, a density $\rho_g = 1{,}2$ kg/m^3 and a kinematic viscosity $\nu_g = 15{,}4 \cdot 10^{-6}$ m^2/s of air were used. The diffusion coefficient was supposed to be $D_g = 13{,}1 \cdot 10^{-6}$m^2/s.

3. Results

The liquid load

$$B = \dot{V}_l / U_W \tag{7}$$

is the liquid flow rate $\dot{V}_l$ divided by the circumference of the wire U_W. The gas load is expressed as F-factor

$$F = v_g \sqrt{\rho_g}\,, \tag{8}$$

whereas v_g is the superficial gas velocity and ρ_g the gas density at system conditions.

3.1. Film thickness

In Fig. 5, the bead thickness (a) and basis film thickness (b) and the frequency of the beads (c) are plotted against the gas load for different liquid loads of water and ethanol. With increasing gas load, the thickness of the beads rises significantly while the basis film thickness remains almost constant. The frequency of the beads is influenced at low liquid loads, the decrease at high gas loads is due to the retardation of the beads by the gas flow. An increase of the liquid flow rises both the bead and basis film thickness and raises the bead frequency. This is an indication, that most of the liquid is transported with the beads at high liquid loads. A comparison of the two liquids shows, that water develops lower basis film and higher bead thicknesses.

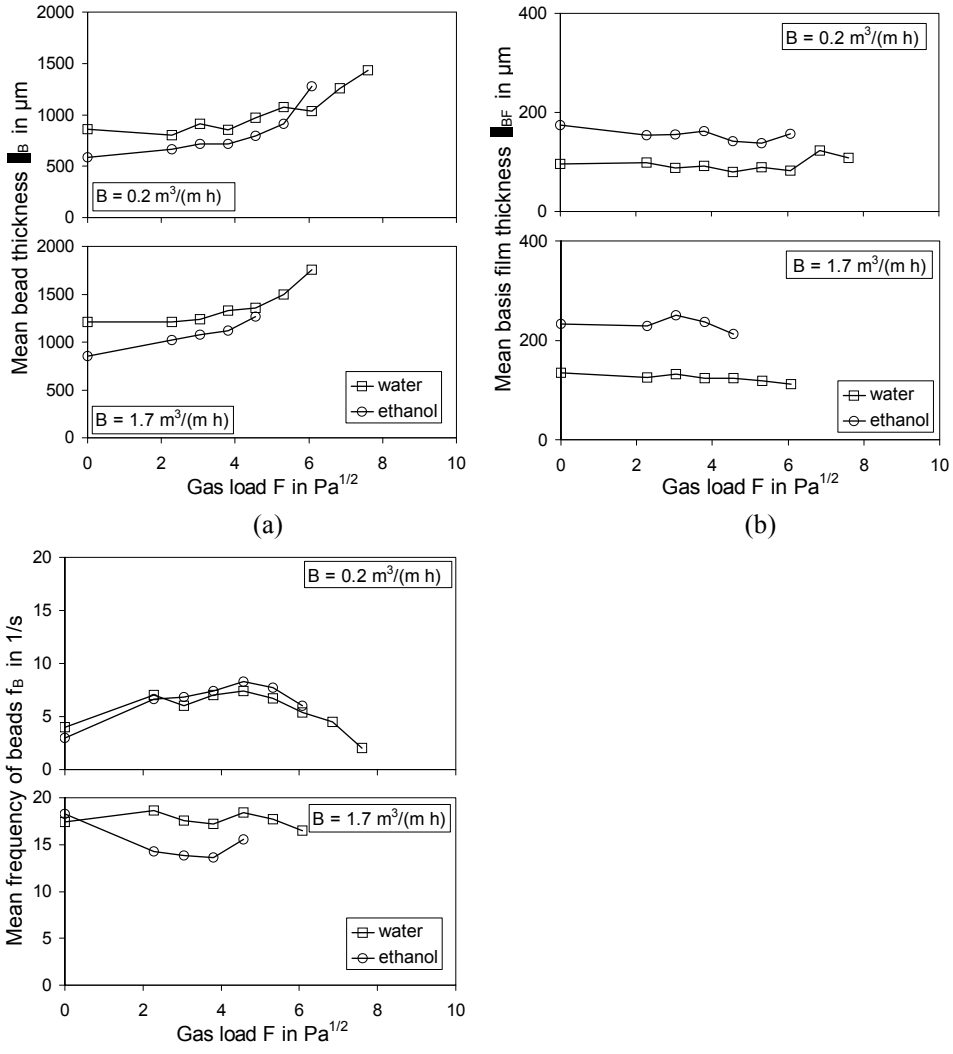

Fig. 5. Bead thickness (a), basis film thickness (b), and frequency of beads (c) depending on gas load

Rys. 5. Wielkość kropli (a), bazowa wielkość kropli (b) i częstość kropli (c) w zależności od wydatku gazu

This can be explained by the higher surface tension of water compared to ethanol, which promotes the formation of beads. Furthermore, the measuring range of water is wider, since the onset of entrainment occurs at higher gas loads. Finally, it is remarkable that the obtained gas loads are higher than the load limits of conventional packings. This is possibly due to the straight gas flow path in the glass channel.

3.2. Gas side mass transfer

A comparison of the experimental data with the empirical correlation of Braun and Hiby (Eq. (5)) is shown in Fig. 6. For both the experiments and empirical correlation, the mass transfer coefficient is rising with increasing gas load and with increasing liquid load. While the dependency of the gas load is comparable, the results show significant difference in the absolute value. One possible reason is the definition of the mass transfer coefficient that is referred to the surface area of the dry wire. Because the ratio of film thickness and wire diameter is large, an increase in film thickness causes a significant enlargement of the liquid surface area, whereas in the case of tubes, the film thickness has almost no geometric influence on the surface area. This could also partially explain the huge influence of the liquid load on the mass transfer. Besides, the increasing frequency of beads at rising liquid loads enhances the mass transfer by promoting the turbulent gas flow and enlarging the surface area of the film.

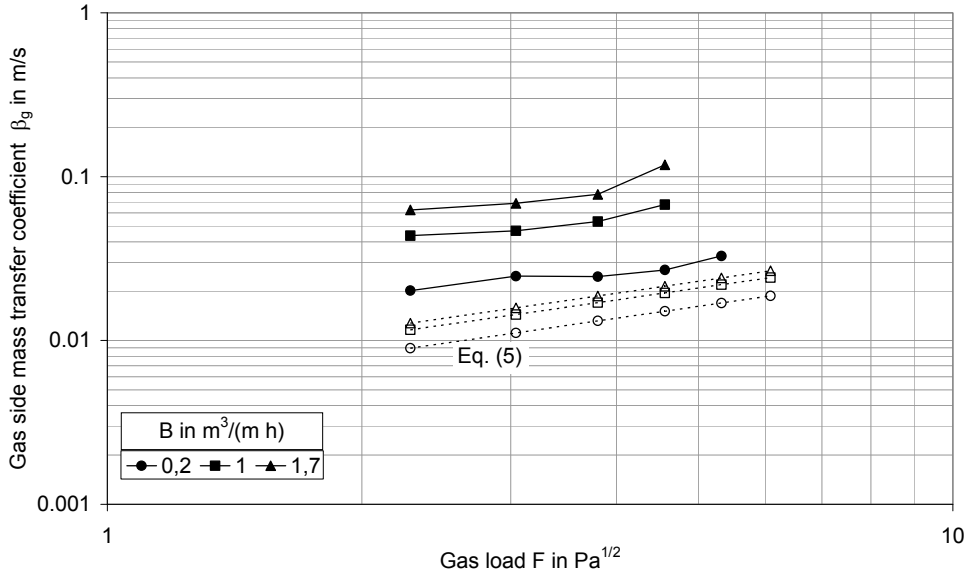

Fig. 6. Gas side mass transfer coefficient, experimental data (solid lines) and empirical correlation Eq. (5), (dashed lines)

Rys. 6. Współczynnik wymiany masy dla gazu; wyniki pomiarów – linie ciągłe i równanie empiryczne (5) – linie przerywane

4. Conclusions

An experimental comparison of the liquids showed a significant influence of the surface tension on the film structure. High surface tension results in larger beads and thinner basis film. A counter current gas flow increases the bead thickness, while it has almost no

influence on basis film thickness. These conclusions have to be considered when designing a wetted-wire column. The mass transfer measurements showed comparatively high transfer coefficients and a considerable dependency on the liquid load, which is different from liquid films on even surfaces.

Symbols

A	– area	[m^2]
B	– liquid load	[m^3/(m h)]
c	– concentration	[mol/m^3]
D	– diffusion coefficient	[m^2/s]
d	– diameter	[m]
F	– gas load	[$Pa^{1/2}$]
f	– frequency	[1/s]
L	– length	[m]
$\tilde{M}$	– molar weight	[kg/kmol]
$\dot{M}$	– mass flow rate	[kg/s]
$\dot{N}$	– molar flow rate	[mol/s]
p	– pressure	[Pa]
R	– universal gas constant	[J/(mol K)]
Re	– Reynolds number	
Sc	– Schmidt number	
Sh	– Sherwood number	
T	– temperature	[K]
U	– circumference	[m]
$\dot{V}$	– volume flow rate	[m^3/s]
v	– superficial velocity	[m^3/(m h)]
β_g	– gas side mass transfer coefficient	[kg/m^3]
δ	– film thickness	[µm]
η	– dynamic viscosity	[kg/(m s)]
ν	– kinematic viscosity	[m^2/s]
ρ	– density	[kg/m^3]
σ	– surface tension	[N/m]

Indices

0	– at the interface	*ln*	– logarithmic
A	– Component *A*	*out*	– outlet
B	– Beads	*s*	– saturation
BF	– Basis film	*T*	– tube
g	– gas	*W*	– wire
l	– liquid		

References

[1] Brauer H.: *Strömung und Wärmeübergang bei Rieselfilmen*, in *VDI-Forsch.-Heft*, VDI-Verlag, Düsseldorf 1956.
[2] Alekseenko S.V., Nakoryakov V.Y., Pokusaev B.G.: AIChE J., **31**, 1985, 1446-1460.
[3] Braun D., Hiby J.W.: Chem. Ing. Tech., **42**, 1970, 345-349.
[4] Ishii M., Grolmes M.A.: AIChE J., **21**, 1975, 308-318.
[5] Wallis G.B.: *One-dimensional Two-phase Flow*, McGraw-Hill, New York 1969.
[6] Mersmann A., Deixler A.: Chem. Ing. Tech., **58**, 1986, 19-31.
[7] Hattori K., Ishikawa M., Mori Y.H.: AIChE J., **40**, 1994, 1983-1992.
[8] Goren S.L.: J. Fluid Mech., **13**, 1962, 309-319.
[9] Lin S.P., Liu W.C.: AIChE J., **21**, 1975, 775-782.
[10] Trifonov Y.Y.: AIChE J., **38**, 1992, 821-834.
[11] Chinju H., Uchiyama K., Mori Y.H.: AIChE J., **46**, 2000, 937-945.
[12] Uchiyama K. et al.: Int. J. Heat Mass Transfer, **46**, 2003, 457-468.
[13] Migita H., Soga K., Mori Y.H.: AIChE J., **51**, 2005, 2190-2198.
[14] *VDI-Wärmeatlas: Berechnungsblätter für den Wärmeübergang*. 7. Auflage, VDI--Verlag, Düsseldorf 1994.
[15] Wohlfarth C., Wohlfarth B.: *Surface Tension of Pure Liquids and Binary Liquid Mixtures*, Landolt-Börnstein – Group IV Physical Chemistry, Springer Verlag, Berlin 1997.
[16] Grünig J., Kraume M., Shilkin A.: Chem. Ing. Tech., **79**, 2007, 1045-1051.
[17] Grünig J. Kraume M., Shilkin A.: Proceedings of the 4th International Berlin Workshop – IBW4 on Transport Phenomena with Moving Boundaries, Berlin, Germany, 2007.
[18] Karimi G., Kawaji M.: Nucl. Eng. Des., **200**, 2000, 95-105.